THE JOURNAL OF PHYSICAL CHEMISTRY B

Article

pubs.acs.org/JPCB

Structural Ensemble of an Intrinsically Disordered Polypeptide

Jeetain Mittal,*[,†,#] Tae Hyeon Yoo,[‡,#] George Georgiou,[§,∥,⊥] and Thomas M. Truskett*[,§]

[†]Department of Chemical Engineering, Lehigh University, Bethlehem, Pennsylvania 18015, United States

[‡]Department of Molecular Science and Technology, Department of Applied Chemistry and Biological Engineering, Ajou University, Suwon 443-749, South Korea

[§]Department of Chemical Engineering, [∥]Department of Biomedical Engineering, [⊥]Section of Molecular Genetics and Microbiology, The University of Texas, 200 East Dean Keeton Street, Stop C0400, Austin, Texas 78712-1589, United States

Supporting Information

ABSTRACT: Intrinsically disordered proteins (IDPs), which play key roles in cell signaling and regulation, do not display specific tertiary structure when isolated in solution. Instead, they dynamically explore an ensemble of unfolded configurations, adopting more stable, ordered structures only after binding to their ligands. Whether ligands induce IDP structural changes upon binding or simply bind to pre-existing conformers that are populated within the IDP's structural ensemble is not well understood. Molecular simulations can provide information with the spatiotemporal resolution necessary to resolve these issues. Here, we report on the conformational ensemble of a 15-residue wild-type p53 fragment from the TAD domain and its mutant (TAD-P27L) obtained by replica exchange molecular dynamics simulation using an optimized (fully atomistic, explicit solvent) protein model and the experimental validation of the simulation results. We use a clustering method based on structural similarity to identify conformer states populated by the peptides in solution from the simulated ensemble. We show that p53 populates solution structures that strongly resemble the ligand (MDM2)-bound structure, but at the same time, the conformational free-energy landscape is relatively flat in the absence of the ligand.

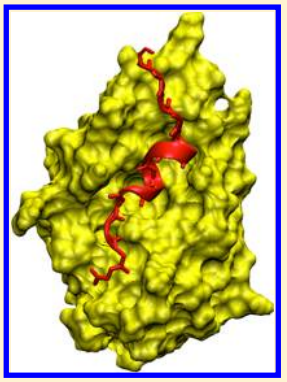

1. INTRODUCTION

Intrinsically disordered proteins (IDPs) do not exhibit stable secondary or tertiary structure under physiological conditions. Instead, they dynamically sample from a diverse ensemble of conformational states.[1−3] Abundant in proteomes across all phyla, IDPs play critical roles in many cellular processes such as signaling and regulation.[4,5] They participate in highly specific but low-affinity binding interactions, often with multiple binding partners such as small molecule or protein ligands.[1,3,6] These properties of IDPs are considered advantageous for dynamic processes requiring both reversibility and specificity within protein−protein interaction networks. Mutations that interfere with the function of IDPs have been predicted to be related to several human pathologies including cancer and cardiovascular disease.[7,8]

Conformational ensembles of IDPs are challenging to characterize experimentally due to their heterogeneous nature. Bioinformatic tools have been developed to identify putative disordered regions in proteins from sequence information. Furthermore, circular dichroism (CD) and nuclear magnetic resonance (NMR) spectroscopy have been used to detect salient structural features of IDPs under various conditions, while NMR and X-ray crystallography have helped to identify specific folded conformations that IDPs adopt upon ligand binding.[9−11] Single-molecule Förster resonance energy transfer (FRET) and fluorescence experiments have been used to probe the dimensions of IDPs and the effect of charged residues on their conformational ensemble under different ionic conditions.[12,13] Nonetheless, successful prediction of how mutations will affect binding affinity and specificity and the detection of minor—but still well populated—conformational states in solution remain formidable challenges. Molecular modeling and simulation techniques can help to address these issues as shown by Sgourakis et al. in their work on Aβ peptides[14,15] and discussed extensively by Chen and co-workers.[16,17] Additionally, several new modeling approaches have been proposed that rely on generating large structural ensembles using simple rules related to volume exclusion and secondary structure propensity[18−22] or coarse-grained polypeptide models.[23] Statistical methods, or so-called restrained molecular simulations, are then utilized to prune and refine the resulting structural ensemble to match experimental observables and thereby to provide insights into populated conformational states.[24−32] Limitations of these approaches are that: (i) multiple nonunique conformational ensembles can match the same experimental data after averaging and, (ii) information about the dynamics of structural rearrangements and the time scales of interconversion between weakly structured states cannot be readily obtained.

p53 is a transcription factor that mediates the response to diverse stresses by regulating many genes related to cell-cycle, apoptosis, senescence, DNA repair, or altered metabolism.[33] Since these functions dictate life or death decisions, the

Received: September 10, 2012
Revised: November 6, 2012

   dx.doi.org/10.1021/jp308984e | J. Phys. Chem. B XXXX, XXX, XXX−XXX

activities of p53 are controlled precisely via interactions with other molecules and via extensive posttranslational modifications.[34] The unstructured N-terminal transactivation domain (TAD) of p53 is at the center of the regulation of the activity of this eminently important transcription factor.[35] The TAD interacts with components of the transcription machinery, the transcription coactivators p300/CBP (CREB-binding protein), and the negative regulators MDM2/MDMX. MDM2 binds to the TAD and simulates p53 degradation and nuclear export acting as a ubiquitin E3 ligase.[36] Structural studies have shown that a short region (residues 15−29) of TAD binds to MDM2 and that in the TAD:MDM2 complex the former assumes a helical conformation.[37,38] Peptides and small molecules mimicking the interaction interface of the TAD inhibit the activity of MDM2 on p53 and stimulate the p53 pathway in tumor cell lines.[39−41]

The goals of the present work are to use a fully atomistic protein model with explicit solvent to accurately predict the equilibrium conformational ensemble of IDPs without resorting to statistics-based ensemble subsampling and reweighting methods and to validate the model using experimental measurements. Replica exchange molecular dynamics (REMD) simulation is used with an optimized protein force field (Amber03w)[42] in conjunction with the accurate TIP4P/2005 water model[43] to identify the structural ensemble of the TAD peptide and a high-affinity variant (TAD-P27L) in solution. TAD-P27L was isolated experimentally by directed evolution of TAD for high affinity binding to MDM2 and shown to display a 150-fold lower equilibrium dissociation constant (K_D). The simulation results are directly validated by comparing to data from NMR spectroscopy experiments. Structural clustering analysis of simulated conformational ensembles shows that residues 19−23 adopt states strikingly similar to those observed in the crystal structure of TAD complexed to MDM2. At the same time, the free-energy surface as a function of root-mean-square deviation (RMSD) from the crystal structure is relatively flat, a result that might be expected—and can be functionally advantageous—for IDPs.

2. RESULTS AND DISCUSSION

Isolation of TAD-P27L and Biophysical Characterization. The N-terminal TAD of p53 (residue 1−73) was displayed on the M13 phage fused to the pIII protein, and its six residues (S20, D21, L22, K24, L25, and P27) were randomized using primers bearing NNK codons (N = A/T/G/C; K = G/T). The generated phage libraries were panned against recombinant MDM2 immobilized on Ni-NAT magnetic beads or Ni-NTA plates following the general phage library screening procedures.[44] After three rounds of panning, around 200 clones were examined for binding to MDM2 using a phage ELISA, and 19 clones showing a signal 40-fold higher than the background (phage displaying TAD) were sequenced (see Table S1 of Supporting Information). Conserved amino acid changes for four positions were identified (S20L, K24E, L25W, and P27L). TAD variants containing each mutation and the TAD-6G1 containing all the mutations combined were examined for binding to MDM2 using ELISA and SPR, and the TAD variant containing theP27L mutation showed the highest binding affinity. TAD (residue 15−29) and TAD-P27L peptides were synthesized by solid phase synthesis, and their binding kinetics to MDM2 were characterized by surface plasmon resonance spectroscopy (see Figure S1 of the Supporting Information). TAD-P27L was shown to exhibit a 150-fold lower equilibrium dissociation constant (K_D) with MDM2, from 2680 nM (TAD) to 18.2 nM (TAD-P27L). Previously, Zondlo et al. reported that a different amino acid substitution at the same position (P27S) also resulted in increased binding to MDM2 albeit with a K_D that was about 4-fold lower than that of TAD-P27L isolated here.[45] Increased binding affinity toward MDM2 is expected to be the result of higher helical propensity[46] induced by replacement of the helix-breaking L-Pro residue by a helix-favoring L-Leu in TAD-P27L or L-Ser amino acid in TAD-P27S.[47]

CD spectra at 298 K (top panel of Figure 1) reveal that, as expected, the TAD peptide lacks significant secondary

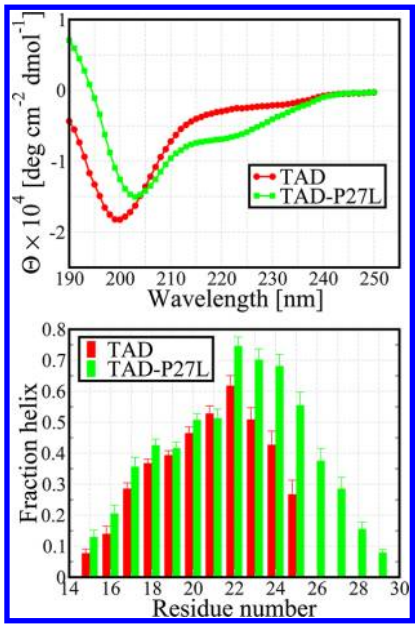

Figure 1. Helical content of TAD and TAD-P27L peptides determined by CD spectroscopy and molecular simulations. (Top) Mean residue ellipticity vs wavelength. (Bottom) Helical fraction vs residue number obtained from replica exchange molecular dynamics simulation at a temperature of 298 K (see Methods section for details).

structure, whereas the TAD- P27L peptide clearly shows a pronounced reduction in molar elipticity at 222 nm characteristic of a helical conformation. Consistent with the CD results, a size exclusion chromatography indicated that TAD-P27L assumes a more compact conformation than the TAD peptide (Figure S2 of the Supporting Information). NMR chemical shift deviations (CSD), relative to random coil, were determined at 298 K on a 600-MHz spectrometer with 1 mM peptides in 90% H_2O/10% D_2O containing 20 mM phosphate (pH 6.0) and 10 mM NaCl (Figure 2).

Molecular Dynamics Simulations. Although predictions of fully atomistic models for well-folded native proteins have been extensively tested,[48−51] the ability of such models to accurately describe structural ensembles of unfolded proteins has yet to be established[20−22] except in very few cases.[14,15] In fact, hybrid methods that make use of available experimental data to direct or reweight the populations of conformational ensembles generated by molecular models are typically employed for the study of IDPs.[19−22,24−32] While hybrid methods ensure some level of consistency with experiments, they also suffer from fundamental limitations. For example, structural populations obtained from hybrid approaches are not unique; i.e., different structural ensembles predict the same

dx.doi.org/10.1021/jp308984e | J. Phys. Chem. B XXXX, XXX, XXX−XXX

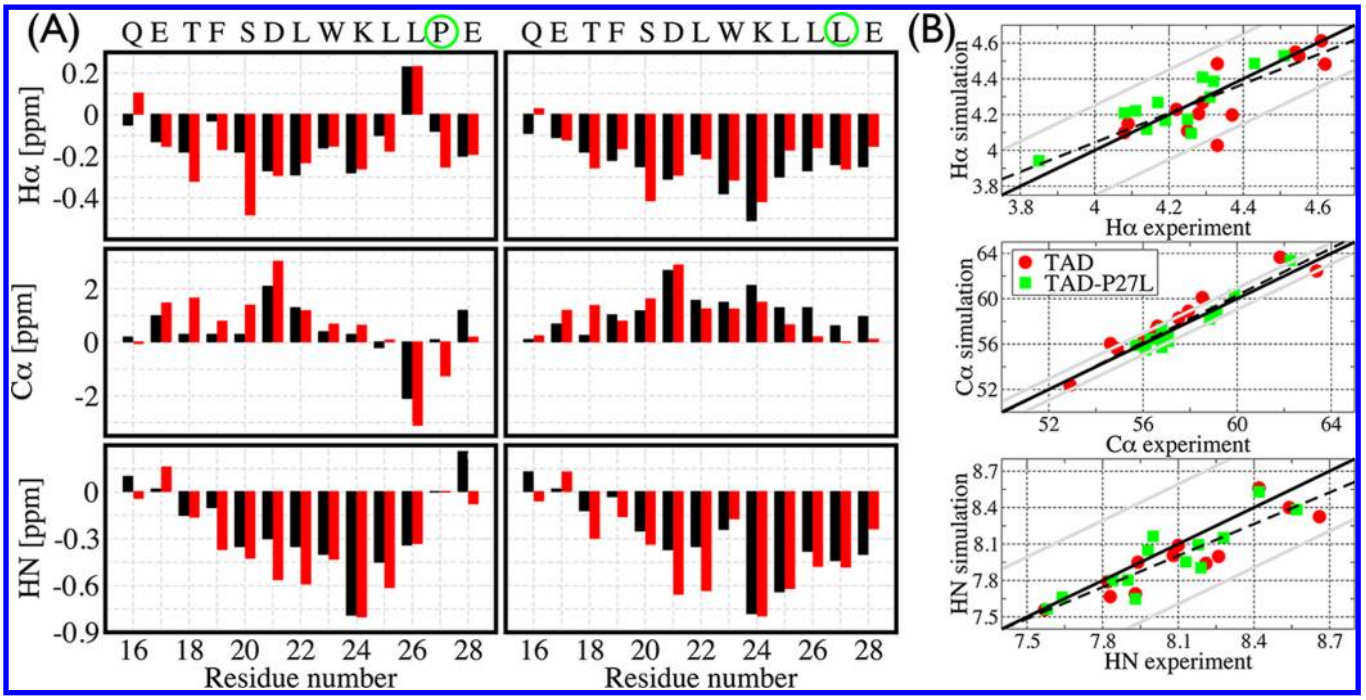

Figure 2. (A) Chemical shift deviations (CSD) relative to random coil values: comparison of data obtained from experiment (black) and simulation (red) for the TAD peptide (left) and the TAD-P27L peptide (right). Experimental and simulation data are represented by black and red bars, respectively. Experimental data is from NMR spectroscopy, and simulation values are from equilibrium REMD configurations analyzed using SPARTA+.[54] (B) Comparison of chemical shift values (in ppm) from NMR experiments to those from the REMD simulated structural ensemble using and SPARTA+. Solid black lines have slopes of unity and intercepts of zero, while the dashed black lines are fits to the data. The solid gray lines represent average accuracy limits of SPARTA+ as discussed by Shen et al.[57]

experimental observables after appropriate averaging. Furthermore, hybrid approaches do not provide a convenient or systematic way to predict the dynamics of IDPs. For these reasons, there is considerable interest in identifying reliable physics-based models that can make direct (unweighted) predictions based solely on knowledge of the amino acid sequence of the polypeptide and the thermodynamic conditions of interest.

Here, we simulate TAD and TAD-P27L fragments using an optimized protein force-field model (Amber03w with TIP4P/2005 explicit water) that has recently been found to reproduce some key experimental trends for unfolded proteins. For example, this model captures how increasing temperature reduces the radius of gyration of unfolded proteins,[42] behavior observed in single-molecule Förster resonance energy transfer (FRET) experiments,[52] but not predicted by other commonly used models. Furthermore, simulations with Amber03w and TIP4P/2005 force fields have been found to reproduce the cooperativity and temperature-dependent carbonyl chemical shifts of the helix−coil transition in helix-forming peptides and to fold model proteins from completely unfolded initial conditions. We believe that the model's ability to treat peptide-solvent interactions, entropic and enthalpic contributions to hydration thermodynamics, and the equation of state of water—as well as to exhibit secondary structure balance (capturing folding behavior of proteins from different structural classes) without ad hoc protein-specific changes in its potential energy function[42]—are critical to its success in describing the properties of unfolded states of proteins, as described below.

To adequately sample configuration space and hence obtain accurate equilibrium properties of IDPs with this atomistic model, REMD simulations—which couple molecular dynamics trajectories with a temperature exchange Monte Carlo process—were employed.[53] In these simulations, dynamics for many replicas of the system are propagated in parallel at different temperatures, spanning from the temperature of interest (298 K) to very high temperatures (590 K) where the system can easily surmount energy barriers separating the various conformational states and hence achieve robust configurational sampling. Periodically, attempts are made to swap the configuration of two replicas and accepted or rejected according to the Metropolis criterion. By following this procedure over the course of a simulation, converged estimations of thermodynamic and structural properties are obtained much more rapidly (independent of the initial conditions employed in the beginning of the simulation as established previously by us and several others[54−56] than with standard molecular dynamics simulations at a single temperature. Full details of our REMD simulations are provided in section 3.3.

From the REMD simulations at 298 K, average helicities (see Methods) of 0.19 and 0.31 are obtained for the TAD and TAD-P27L peptides, respectively. The average helical segment lengths (and numbers of such helical segments) are found to be 3.25 (0.78) and 3.8 (1.06) for TAD and TAD-P27L, respectively. The simulations also provide residue-specific peptide helicity propensities, as shown in Figure 1 (bottom panel). From this data, we find that the proline to leucine substitution at position 27 does not affect the helicity of residues 15−21 but significantly enhances the helicity of C-terminal residues 22−29. This observation is consistent with the experimental trends reported by Zondlo et al.,[45] who used CD and NMR spectroscopies to demonstrate that the p53 TAD peptide comprising residues 17−29 has substantially less

dx.doi.org/10.1021/jp308984e | J. Phys. Chem. B XXXX, XXX, XXX−XXX

α-helicity than its mutant formed by a proline to serine substitution at position 27.

Simulation of NMR CSD data were obtained from REMD using SPARTA+,[57] a well-tested CSD computation tool based on an artificial neural-network algorithm, which empirically but accurately evaluates inputted equilibrium peptide conformations against a large protein database to predict chemical shifts. As is evident in Figure 2A, there is very good agreement between the data from the experiments and the simulated atomistic model. Both data sets show a clear increase in TAD-P27L peptide helicity at the C-terminal as compared to the TAD peptide (the positive values of Ca and the negative values of Ha and HN CSD are empirically known to correspond to more helical structures[59,60]), results consistent with the simulated helicities and CD data of Figure 1 discussed earlier. This correspondence between simulation and experiments further demonstrates that the present atomistic model can directly reproduce subtle residue-specific information about TAD peptide structure in solution, including point mutation effects. We quantify the deviations between experimental and simulation values by calculating the root-mean-square deviation (RMSD). We find the RMSD numbers (in ppm) to be 0.09 (Hα), 0.88 (Cα), and 0.14 (HN) for TAD and 0.08 (Hα), 0.54 (Cα), and 0.13 (HN) for TAD-P27L. The maximum RMSD (in ppm) observed for a residue is 0.30 (Hα), 1.83 (Cα), and 0.34 (HN) for TAD and 0.16 (Hα), 1.12 (Cα), and 0.28 (HN) for TAD-P27L in units of ppm. These RMSD numbers are within the accuracy limits (0.25 (Hα), 0.94 (Cα), and 0.49 (HN)) of the shift prediction algorithm used here, i.e., SPARTA+.[57] The NMR data based on p53 TAD fragment (residues 15−29) is also consistent with the full-length p53 TAD peptide (73 residues) for the same residues (see Figure S3 of the Supporting Information) as reported earlier by Lee et al.[58]

To characterize the peptide conformations populated in the equilibrium ensemble, we use a structure-based clustering algorithm.[61] The algorithm sorts peptide conformers into clusters based on their structural similarity; in this case, measured by backbone root-mean-square distance (RMSD). Residues 18−26, expected to be structured in the MDM2 bound state,[38] are used to measure RMSD. Figure 3 shows the most populated clusters for the two peptides. Interestingly, these structures represent a significant fraction of the sampled equilibrium conformations (54% and 66% for TAD and TAD-P27L, respectively), a counterintuitive result given that IDPs are not expected a priori to form stable structures in the absence of a binding partner. However, examination of the individual conformations contained in these highly populated clusters reveals that there is still significant structural disorder present at both N- and C-termini.

To clarify this point, we obtain a separate set of clusters based on the backbone RMSD of all the peptide residues (15−29). The resulting clusters are shown in Figure S4 of the Supporting Information. In this case, the fraction of conformations in each cluster (including the most populated cluster) is small and consistent with expectations for an IDP's structural ensemble. A comparison between clustering results based on 18−26 residues and 15−29 residues therefore highlights an important point: even though neither peptide forms long stretches of stable secondary structure, the majority of conformations display short stretches of specific and stable secondary structure. Experimentally, some of these structures may be challenging to detect using standard biophysical

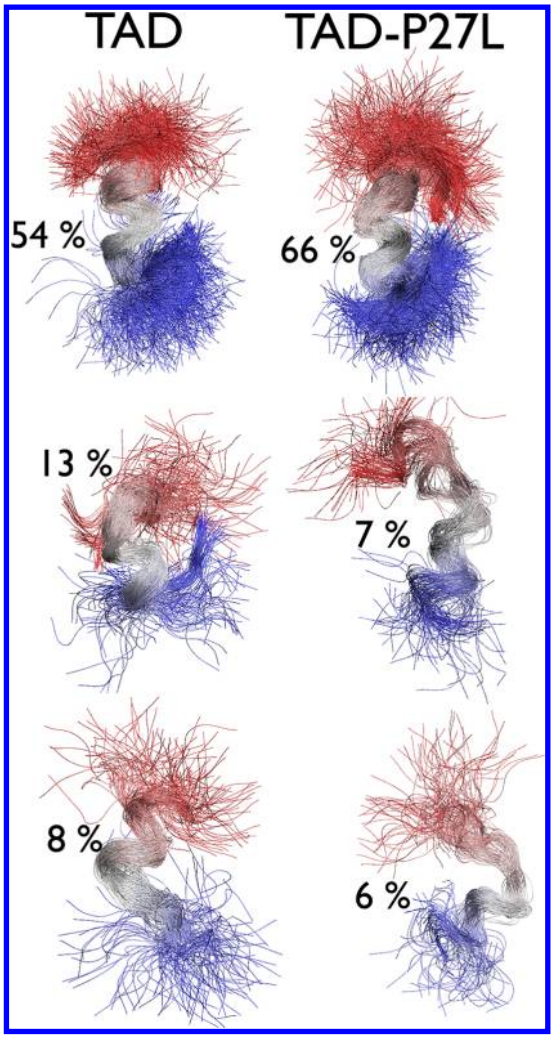

Figure 3. Representative structures from the five most populated clusters (% population indicated) obtained from simulation of the TAD peptides in solution are shown. The calculations are based on backbone atoms only and include residues T18−L26.

techniques due to weak signal but still might have significant functional relevance (e.g., peptide interactions with binding target), reinforcing the need for predictive atomistic models. In the case of TAD peptides, interactions between TAD-MDM2 are thought to be facilitated by such structures, i.e., "conformational selection".[62] At the same time, some aspects of the binding mechanism likely have elements of "induced fit" because conformational heterogeneity at the N- and C-termini can potentially be attenuated in the presence of a binding partner; a prediction from this work that can be tested in future studies.

We also investigated whether the structural motifs that the TAD peptides display when isolated in solution are similar to the MDM2-bound states, and we also characterized the shape of the free-energy landscape corresponding to the peptides' conformational ensembles. Figure 4 shows the computed one-dimensional free-energy surface projected as a function of the backbone RMSD relative to the MDM2-bound crystal structure of (PDB ID: 1YCR) for both the TAD peptide and TAD-P27L. As several residues are either unresolved or disordered in the crystal structure,[36] we only include residues 18 to 26 in our calculation. One striking point is that the free-energy profile is virtually flat for the TAD peptide between RMSD values 0.1

dx.doi.org/10.1021/jp308984e | J. Phys. Chem. B XXXX, XXX, XXX−XXX

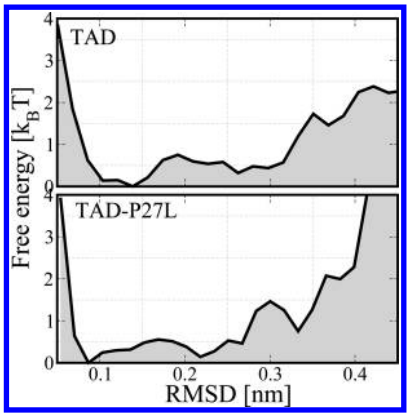

Figure 4. Free-energy landscapes of the peptides are shown, as characterized by the potential of mean force projected onto the root mean-square distance (RMSD) relative to the MDM2 bound structure (PDB: 1YCR). Calculations are based on backbone atoms only and include residues T18−L26 as other residues are either not resolved in the crystal structure or disordered. On the basis of a cutoff of 0.2 nm, the population is about 50% in the native state.

and 0.3 nm. In fact, even configurations relatively far from the native MDM2-bound state (RMSD > 0.3 nm) have free-energy differences of <2.5 k_BT compared to the most stable configuration (RMSD ≈ 0.15). This suggests that the equilibrium structural ensemble of both the TAD peptide and TAD-P27L are very flexible and thus conformations should be able to rapidly interconvert. In case of IDPs, this can be advantageous for their biological function as proposed by Shoemaker et al. in the fly casting mechanism of molecular recognition.[63] They found that disordered proteins have a greater capture radius for their ligands as opposed to folded domains with limited flexibility. In the case of TAD peptides considered here, significant disorder at the N- and C- termini can therefore facilitate initial binding steps (kinetically controlled) to MDM2.

Interestingly, the free-energy surface of TAD-P27L is also virtually flat across a wide range of backbone RMSDs as shown in Figure 4 (bottom panel). As the crystal structure for MDM2-bound TAD-P27L is not available, we use the TAD-MDM2 crystal structure as the reference here as well. On the basis of RMSD of common residues 18−26, we do not find significant differences in the free-energy surfaces of the two peptides. This is consistent with our experimental binding rate data from which we find that the TAD and TAD-P27L peptides have similar on rates ($k_{on}^{WT}/k_{on}^{P27L} \approx 0.2$). The 5-fold difference may be attributable in part to the subtle differences in solution structure between the TAD-P27L and TAD peptides discussed earlier. At the same time, our experiments show significantly different off rates ($k_{off}^{WT}/k_{off}^{P27L} \approx 30$), perhaps suggesting that the peptides exhibit disparate structures (helicities) in their MDM2-bound conformations.

3. CONCLUDING REMARKS

The present study demonstrates that experimentally validated, residue-specific structural information about IDPs in solution, including the effects of point mutations, can be obtained from simulations of an atomistic explicit-solvent model optimized to reproduce protein−solvent interactions and the thermodynamics of water. The simulated structural ensembles for a 15-residue wild-type p53 fragment and its mutant (P27L) in solution are shown to contain conformers with striking similarity to their corresponding MDM2-bound structures, in accordance with expectations from a pre-equilibrium binding mechanism. The similarities come from short stretches of stable secondary structure that are present in the central region of the peptides. Both N- and C-termini are disordered in the peptides' structural ensembles, and their free-energy landscapes are relatively flat. These features indicate that the peptides can rapidly interconvert between conformations, flexibility that might be important for their biological function. The success of this atomistic model opens the door for future studies, including characterization of the dynamics of TAD peptides and study of their structural ensembles in the presence of MDM2.

4. MATERIALS AND METHODS

3.1. Peptides. Peptides were synthesized with >98% purity at ABGENT (San Diego, California). The N-termini and C-termini were acetylated and amidated, respectively. The sequence of the TAD peptide is Ac-SQETFSDLWKLLPEN-CONH2, and that of the P27L peptide is Ac-SQETFSDLWKLLLEN-CONH2 (the amino acid change in P27L with respect to TAD is underlined).

3.2. CD and NMR Spectroscopy. CD spectra were collected at 298 K on a Jasco J-815 CD Spectrometer (Easton, Maryland) in a 1-mm cell with 75 μM peptide in 5 mM phosphate buffer (pH 7.0) containing 25 mM KF, following the published method.[42] NMR spectra were collected at 298 K on a Varian DirectDrive 600 MHz spectrometer (Vernon Hills, Illinois) with 1 mM peptides in 90% H_2O/10% D_2O containing 20 mM phosphate (pH 6.0) and 10 mM NaCl, again according to the published procedure.[45]

3.3. Simulation Details. The Amber ff03w force field[42] (Amber ff03 (64) with a modified Ψ torsion potential) with the TIP4P/2005 model for water[43] is used to model the peptide in solution. The peptides are solvated in a truncated octahedron simulation cell with 4 nm between the nearest faces, using 1522 water molecules, 8 sodium ions, and 6 chloride ions to neutralize the charge. Replica exchange molecular dynamics[65] simulations are performed in the NVT ensemble. 36 replicas, spanning the temperature range from 278 to 590 K, are simulated. The temperatures (in K) used are: 278, 283, 288, 293, 298, 303, 308, 313, 318, 324, 330, 337, 344, 352, 360, 369, 378, 388, 398, 409, 420, 431, 444, 455, 466, 477, 488, 499, 510, 521, 532, 543, 554, 566, 578, and 590. The systems are propagated using Langevin dynamics with a friction of 1 ps^{-1}. The particle mesh Ewald method[66] is used to calculate electrostatic interactions with a real space cutoff of 0.9 Å. The cutoff for van der Waals interactions are taken to be 1.4 Å. Each replica is simulated for 200 ns with a time step of 2 fs, and the initial 30 ns are discarded as equilibration. This simulation time is much longer than found necessary for a longer IDP (40−42 residues) in previous work by Garcia and co-workers and is used to minimize sampling artifacts.[14,15] All simulations are performed using GROMACS 4.0.7.[67,68]

We have used a dihedral-based method to assign residue-level helicity. The α_h region of the (φ, ψ) map is defined as $\varphi \in [-100°, -30°]$ and $\psi \in [-67°, -7°]$. Residues that lie within the α_h region of the Ramachandran map are denoted as helical (h). All residues outside the α_h region are defined as "coil" (c). A helical segment is one that has at least three consecutive residues with (φ, ψ) angles that fall within the α_h boundaries. The fraction of helix for a given residue in the simulation is

dx.doi.org/10.1021/jp308984e | J. Phys. Chem. B XXXX, XXX, XXX−XXX

calculated as the fraction of time spent by that residue within helical segments.

■ ASSOCIATED CONTENT

Supporting Information

Table with amino acid sequences of isolated TAD variants from phage display. Figures showing kinetic analysis by surface plasmon resonance, size exclusion chromatography, chemical shift comparison, structural clustering. This information is available free of charge via the Internet at http://pubs.acs.org.

■ AUTHOR INFORMATION

Corresponding Author

*E-mail: jeetain@lehigh.edu (J.M.); ttruskett@utexas.edu (T.T.).

Author Contributions

#These authors contributed equally to this work.

Notes

The authors declare no competing financial interest.

■ ACKNOWLEDGMENTS

This study utilized the high-performance computational capabilities of the Biowulf PC/Linux cluster at the National Institutes of Health, Bethesda, MD (http://biowulf.nih.gov). T.M.T. acknowledges support of the Welch Foundation (F-1696) and the National Science Foundation (CBET-1065357). G.G. acknowledges support from Grant No. N00014-09-1-1087 from ONR. T.H.Y. acknowledges support of the Mid-Career Research Program (2012-016803) and the Priority Research Program (2012-0006687) through the National Research Foundation (NRF) funded by the Ministry of Education, Science and Technology. We would like to thank Steve Sorey at the NMR facility of the University of Texas at Austin for help with the NMR analysis.

■ REFERENCES

(1) Dyson, H. J.; Wright, P. E. *Nat. Rev. Mol. Cell Biol.* **2005**, *6*, 197−208.
(2) Tompa, P. *FEBS Lett.* **2005**, *579*, 3346−3354.
(3) Uversky, V. N. *Protein Sci.* **2002**, *11*, 739−756.
(4) Cheng, Y.; LeGall, T.; Oldfield, C. J.; Mueller, J. P.; Van, Y.-Y. J.; Romero, P.; Cortese, M. S.; Uversky, V. N.; Dunker, A. K. *Trends Biotechnol.* **2006**, *24*, 435−442.
(5) Ward, J.; Sodhi, J.; McGuffin, L.; Buxton, B.; Jones, D. *J. Mol. Biol.* **2004**, *337*, 635−645.
(6) Tompa, P.; Fuxreiter, M. *Trends Biochem. Sci.* **2008**, *33*, 2−8.
(7) Cheng, Y.; LeGall, T.; Oldfield, C.; Dunker, A. K.; Uversky, V. N. *Biochemistry* **2006**, *45*, 10448−10460.
(8) Iakoucheva, L.; Brown, C.; Lawson, J.; Obradovic, Z.; Dunker, A. K. *J. Mol. Biol.* **2002**, *323*, 573−584.
(9) Bracken, C.; Iakoucheva, L.; Romero, P.; Dunker, K. A. *Curr. Opin. Struct. Biol.* **2004**, *14*, 570−576.
(10) Radivojac, P.; Iakoucheva, L. M.; Oldfield, C. J.; Obradovic, Z.; Uversky, V. N.; Dunker, A. K. *Biophys. J.* **2007**, *92*, 1439−1456.
(11) Receveur-Bréchot, V.; Bourhis, J.; Uversky, V. N.; Canard, B.; Longhi, S. *Proteins* **2006**, *62*, 24−45.
(12) Müller-Späth, S.; Soranno, A.; Hirschfeld, V.; Hofmann, H.; Rüegger, S.; Reymond, L.; Nettels, D.; Schuler, B. *Proc. Natl. Acad. Sci. U.S.A.* **2010**, *107*, 14609.
(13) Mao, A. H.; Crick, S. L.; Vitalis, A.; Chicoine, C. L.; Pappu, R. V. *Proc. Natl. Acad. Sci. U.S.A.* **2010**, *107*, 8183.
(14) Sgourakis, N. G.; Yan, Y. L.; McCallum, S. A.; Wang, C. Y.; Garcia, A. E. *J. Mol. Biol.* **2007**, *368*, 1448.
(15) Sgourakis, N. G.; Merced-Serrano, M.; Boutsidis, C.; Drineas, P.; Du, Z.; Wang, C.; Garcia, A. E. *J. Mol. Biol.* **2011**, *405*, 570.
(16) Click, T. H.; Ganguly, D.; Chen, J. *Int. J. Mol. Sci.* **2010**, *11*, 5292−5309.
(17) Chen, J. *Arch. Biochem. Biophys.* **2012**, *524*, 123−131.
(18) Jha, A.; Colubri, A.; Freed, K. F.; Sosnick, T. R. *Proc. Natl. Acad. Sci. U.S.A.* **2005**, *102*, 13099−13104.
(19) Wells, M.; Tidow, H.; Rutherford, T. J.; Markwick, T. J.; Jensen, M. R.; Mylonas, E.; Svergun, D. I.; Blackledge , M.; Fersht, A. R. *Proc. Natl. Acad. Sci. U.S.A.* **2008**, *105*, 5762.
(20) Mittag, T.; Forman-Kay, J. *Curr. Opin. Struct. Biol.* **2007**, *17*, 3−14.
(21) Ringkjobing Jensen, M.; Markwick, P. R. L.; Meier, S.; Griesinger, C.; Zweckstetter, M.; Grzesiek, S.; Bernado, P.; Blackledge, M. *Structure* **2009**, *17*, 1169−1185.
(22) Fisher, C.; Stultz, C. *Curr. Opin. Struct. Biol.* **2011**, *21*, 426−431.
(23) Ashbaugh, H. S.; Hatch, H. W. *J. Am. Chem. Soc.* **2008**, *130*, 9536.
(24) Dedmon, M. M.; Lindorff-Larsen, K.; Christodoulou, J.; Vendruscolo, M.; Dobson, C. M. *J. Am. Chem. Soc.* **2005**, *127*, 476−477.
(25) Francis, C. J.; Lindorff-Larsen, K.; Best, R. B.; Vendruscolo, M. *Proteins* **2006**, *65*, 145−152.
(26) Lowry, D.; Stancik, A.; Shrestha, R.; Daughdrill, G. *Proteins* **2008**, *71*, 587−598.
(27) Huang, J.; Grzesiek, S. *J. Am. Chem. Soc.* **2009**, *132*, 694−705.
(28) Esteban-Martìn, S.; Fenwick, R.; Salvatella, X. *J. Am. Chem. Soc.* **2010**, *132*, 4626−4632.
(29) Fisher, C.; Huang, A.; Stultz, C. *J. Am. Chem. Soc.* **2010**, *132*, 14919−14927.
(30) Marsh, J.; Forman-Kay, J. *Proteins* **2012**, *80*, 556−572.
(31) Ytreberg, F. M.; Zuckerman, D. M. *Proc. Natl. Acad. Sci. U.S.A.* **2008**, *105*, 7982−7987.
(32) Daughdrill, G. W.; Kashtanov, S.; Stancik, A.; Hill, S. E.; Helms, G.; Muschol, M.; Receveur-Brechot, V.; Ytreberg, F. M. *Molecular BioSystems* **2012**, *8*, 308.
(33) Vousden, K.; Lane, D. *Nat. Rev. Mol. Cell Biol.* **2007**, *8*, 275−283.
(34) Brooks, C.; Gu, W. *Mol. Cell* **2006**, *21*, 307−315.
(35) Toledo, F.; Wahl, G. *Nat. Rev. Canc.* **2006**, *6*, 909−923.
(36) Chène, P. *Nat. Rev. Cancer* **2003**, *3*, 102−109.
(37) Joerger, A.; Fersht, A. *Annu. Rev. Biochem.* **2008**, *77*, 557−582.
(38) Kussie, P.; Kussie, P.; Gorina, S.; Marechal, V.; Elenbaas, B.; Moreau, I.; Levine, A. I.; Pavletich, N. P. *Science* **1996**, *274*, 948−953.
(39) Issaeva, N.; Bozko, P.; Enge, M.; Protopopova, M.; Verhoef, L. G.; Masucci, M.; Pramanik, A.; Selivanova, G. *Nat. Med.* **2004**, *10*, 1321−1328.
(40) Shangary, S.; Qin, D.; McEachern, D.; Liu, M.; Miller, R. S.; Qiu, S.; Nikolovska-Coleska, Z.; Ding, K.; Wang, G.; Chen, J.; Bernard, D.; Zhang, J.; Lu, Y.; Gu, Q.; Shah, R. B.; Pienta, K. J.; Ling, X.; Kang, S.; Guo, M.; Sun, Y.; Yang, D.; Wang, S. *Proc. Natl. Acad. Sci. U.S.A.* **2008**, *105*, 3933.
(41) Vassilev, L.; Vu, B. T.; Graves, B.; Carvajal, D.; Podlaski, F.; Filipovic, Z.; Kong, N.; Kammlott, U.; Lukacs, C.; Klein, C.; Fotouhi, N.; Liu, E. A. *Science* **2004**, *303*, 844.
(42) Best, R. B.; Mittal, J. *J. Phys. Chem. B* **2010**, *114*, 14916.
(43) Abascal, J. L. F.; Vega, C. *J. Chem. Phys.* **2005**, *123*, 234505.
(44) Barbas, C. F.; Burton, D. R.; Scott, J. K.; Silvermann, G. J. *Phage Display: A Laboratory Manual*; Cold Spring Harbor Laboratory Press, Cold Spring Harbor, NY, 2001.
(45) Zondlo, S.; Lee, A.; Zondlo, N. *Biochemistry* **2006**, *45*, 11945−11957.
(46) Dastidar, S.; Lane, D.; Verma, C. *J. Am. Chem. Soc.* **2008**, *130*, 13514−13515.
(47) Nick Pace, C.; Martin Scholtz, J. *Biophys. J.* **1998**, *75*, 422−427.
(48) Paschek, D.; Hempel, S.; Garcia, A. E. *Proc. Natl. Acad. Sci. U.S.A.* **2008**, *105*, 17754.
(49) Freddolino, P.; Harrison, C.; Liu, Y.; Schulten, K. *Nature Physics* **2010**, *6*, 751−758.
(50) Mittal, J.; Best, R. B. *Biophys. J.* **2010**, *98*, 1−3.

(51) Piana, S.; Lindorff-Larsen, K.; Shaw, D. E. *Biophys. J.* **2011**, *100*, 47.
(52) Nettels, D.; Muller-Spath, S.; Kuster, F.; Hofmann, H.; Haenni, D.; Ruegger, S.; Reymond, L.; Hoffmann, A.; Kubelka, J.; Heinz, B.; Gast, K.; Best, R. B.; Schuler, B. *Proc. Natl. Acad. Sci. U.S.A.* **2009**, *106*, 20740.
(53) Earl, D. J.; Deem, M. W. *Phys. Chem. Chem. Phys.* **2005**, *7*, 3910.
(54) Best, R. B.; Mittal, J. *J. Phys. Chem. B* **2010**, *114*, 8790.
(55) Day, R.; Paschek, D.; Garcia, A. E. *Proteins* **2010**, *78*, 1889.
(56) Lin, E.; Shell, M. S. *J. Chem. Theory Comput.* **2009**, *5*, 2062.
(57) Shen, Y.; Bax, A. *J. Biomol. NMR* **2010**, *48*, 13−22.
(58) Lee, H.; Hun Mok, K.; Muhandiram, R.; Park, K.-H.; Suk, J.-E.; Kim, D.-H.; Chang, J.; Chul Sung, Y.; Choi, K. Y.; Han, K.-H. *J. Biol. Chem.* **2000**, *275*, 29426−29432.
(59) Spera, S.; Bax, A. *J. Am. Chem. Soc.* **1991**, *113*, 5490−5492.
(60) Wishart, D.; Sykes, B.; Richards, F. *J. Mol. Biol.* **1991**, *222*, 311−333.
(61) Daura, X.; Gademann, K.; Jaun, B.; Seebach, D.; van Gunsteren, W. F.; Mark, A. E. *Angew. Chem., Int. Ed.* **1999**, *38*, 236−240.
(62) Boehr, D.; Nussinov, R.; Wright, P. *Nat. Chem. Biol.* **2009**, *5*, 789−796.
(63) Shoemaker, B. A.; Portman, J. J.; Wolynes, P. G. *Proc. Natl. Acad. Sci. U.S.A.* **2000**, *97*, 8868.
(64) Duan, Y.; Wu, C.; Chowdhury, S.; Lee, M. C.; Xiong, G.; Zhang, W.; Yang, R.; Cieplak, P.; Luo, R.; Lee, T.; Caldwell, J.; Wang, J.; Kollman, P. *J. Comput. Chem.* **2003**, *24*, 1999−2012.
(65) Sugita, Y.; Okamoto, Y. *Chem. Phys. Lett.* **1999**, *314*, 141−151.
(66) Essmann, U.; Perera, L.; Berkowitz, M. L.; Darden, T.; Lee, H.; Pedersen, L. G. *J. Chem. Phys.* **1995**, *103*, 8577.
(67) Berendsen, H. J. C.; van der Spoel, D.; van Drunen, R. *Comput. Phys. Commun.* **1995**, *91*, 43−56.
(68) Hess, B.; Kutzner, C.; van der Spoel, D.; Lindahl, E. *J. Chem. Theory Comput.* **2008**, *4*, 435−447.